Supporting Information: Thermophysical properties of adsorbates with beyond-DFT accuracy from DFT data through error cancellation

Seth Porter and Bjarne Kreitz*

School of Chemical and Biomolecular Engineering, Georgia Institute of Technology, Atlanta, GA 30332, USA

E-mail: bkreitz3@gatech.edu

1 Experimental Data

Enthalpies of formation of the adsorbates that are used as reference species for the CBH scheme are derived from experimental measurements. These measurements include single-crystal adsorption calorimetry (SCAC) or temperature-programmed desorption (TPD). The quantity that is measured is either the heat of adsorption (in the SCAC) or the desorption energy, from which the heat of desorption can be easily derived for non-activated adsorption processes. The derivation of the enthalpies of formation from the measured heats of adsorption is straightforward and is briefly described. For an associative adsorption of a molecule X on a metal surface (denoted as $*$) with the following reaction equation

$$\mathrm{X} + * \rightleftharpoons \mathrm{X}*$$

We can calculate the enthalpy of formation of the adsorbate X$*$ easily from the heat of adsorption $\Delta H_{\mathrm{ads}}(T_{\mathrm{exp}})$ and the enthalpy of formation of the species in the gas phase $\Delta_{\mathrm{f}}H_{\mathrm{X}}^{\mathrm{ATcT}}(T_{\mathrm{exp}})$, which can typically be obtained from the Active Thermochemical Tables (ATcT).

$$\Delta_{\mathrm{f}}H_{\mathrm{X}*}(T_{\mathrm{exp}}) = \Delta H_{\mathrm{ads}}(T_{\mathrm{exp}}) + \Delta_{\mathrm{f}}H_{\mathrm{X}}^{\mathrm{ATcT}}(T_{\mathrm{exp}}) + \Delta_{\mathrm{f}}H_{*} \tag{1}$$

The enthalpy of formation of the single crystal metal surface $\Delta_f H_*$, e.g., Pt(111), is defined to be $0\,\mathrm{kJ\,mol^{-1}}$. Heats of adsorption are measured at a specific temperature T_{exp}. To evaluate the enthalpy of formation of the adsorbate at this temperature, it is necessary to convert the enthalpy of formation of the gas-phase reference species to T_{exp}, which can be done using the NASA polynomials of the gas-phase species.

$$\Delta_f H_X^{ATcT}(T_{exp}) = \Delta_f H_X^{ATcT}(298K) - [H_{298K} - H_{Texp}](X) \quad (2)$$

The enthalpy of formation of the adsorbate can then be determined at T_{exp} and corrected to the typical reference temperature of 298 K commonly used for thermochemical values. Partition functions of the adsorbed species are used to calculate the term $[H_{298K} - H_{Texp}](X*)$ (the integrated molar heat capacity), which are derived from the vibrational modes using the harmonic oscillator approximation.

$$\Delta_f H_{X*}(298K) = \Delta_f H_{X*}(T_{exp}) - [H_{298K} - H_{Texp}](X*) \quad (3)$$

Electronic structure calculations are always carried out at a temperature of 0 K. Thus, to use the experimental enthalpies of formation of the reference species in the error cancellation reactions, it is necessary to derive the enthalpy of formation at 0 K from the enthalpy of formation at 298 K via Equation (4).

$$\Delta_f H_{X*}(0K) = \Delta_f H_{X*}(298K) - [H_{298K} - H_{0K}](X*) + \sum_{j=1}^{n} [H_{298K} - H_{0K}](\mathrm{element_j}) \quad (4)$$

NASA polynomials of the species cannot be used since they are not valid close to 0 K. Enthalpy increments of the elements $[H_{298K} - H_{0K}](\mathrm{element_j})$ were taken from S1 and are reported in Table S1.

Table S1: Enthalpy increments of the elements in $\mathrm{kJ\,mol^{-1}}$ from the Active Thermochemical Tables (ATcT).[S1]

species	$[H_{298K} - H_{0K}]$
H	4.234
O	4.340
C	1.051

1.1 Correction of the experimental values for methoxy on Pt(111) and Ni(111)

Enthalpies of adsorption of methoxy on Pt(111) and Ni(111) were measured via single-crystal adsorption calorimetry by Campbell and co-workers.[S2,S7] These enthalpies were determined

Table S2: Measured heats of adsorption on Pt(111) and derived enthalpies of formation at 0 K for the species that were used as fragments for the bond types to construct the CBH reactions. All enthalpies are in kJ mol^{-1}.

species	bond type	reaction	ΔH_{ads}	T (K)	$\Delta_{\mathrm{f}}H^{\mathrm{exp}}_{0\mathrm{K}}$	ref.
CH_3OH*	C–O	$CH_3OH(g) + * \rightleftharpoons CH_3OH*$	-263	100	-245.0	S2
H_2CO*	C=O	$H_2CO(g) + * \rightleftharpoons H_2CO*$	-55.2	235	-159.3	S3
CH_3CH_3*	C–C	$CH_3CH_3(g) + * \rightleftharpoons CH_3CH_3*$	-28.5	106	-96.0	S4
CH_4*	C–H	$CH_4(g) + * \rightleftharpoons CH_4*$	-15	63	-81.3	S4
H_2O*	O–H	$H_2O(g) + * \rightleftharpoons H_2O*$	-31.3	120	-267.9	S4
$*OH^b$	Pt–O	$H_2O* + * \rightleftharpoons *OH + *H$	68	298	-164.7	S5

[b] The enthalpy of formation of ∗OH was calculated from an experimental reaction enthalpy taken from Karp et al.[S5]

[c] The measured heat of adsorption of these reactions was corrected by 2 kJ mol^{-1} compared to the original paper due to a systematic error as described in ref. S6.

by measuring the adsorption of methanol on ∗O- precovered Ni(111) or Pt(111) surfaces, leading to methanol dissociation and the formation of $*OCH_3$. The integral enthalpies of adsorption reported in the original manuscripts by Karp et al.[S2] and Carey et al.[S7] are at a coverage of 1/4 ML of methoxy and 1/4 ML of ∗O. Thus, the overall coverage of the (111) facet is 1/2 ML. A strong coverage dependence of the heat of adsorption is observed in the experiments for methoxy. Additionally, ∗O also shows strong repulsive interactions on Pt(111)[S8] and Ni(111),[S9] which lead to a destabilization of the adsorbates. Therefore, we can hypothesize that there are also repulsive interactions between $*OCH_3$ and ∗O.

DFT calculations with the BEEF-vdW exchange-correlation functional for methoxy are performed with one $*OCH_3$ per (3×3) cell, corresponding to a coverage of 1/9 ML. For a fair comparison of experiments and theory, it is necessary to use the same adsorbate coverage for both. We used the provided relations for the differential enthalpy of adsorption for Pt(111) and Ni(111) to determine the integral heat of adsorption for a total coverage of 1/9 ML (1/18 ML methoxy and 1/18 ML hydroxyl).

$$\Delta H_{\mathrm{ads}} = 85.5\,\mathrm{kJ\,mol^{-1}} - 72.1\,\mathrm{kJ\,mol^{-1}}\theta_{*\mathrm{OCH_3}} \qquad \text{for Pt(111)} \tag{5}$$

$$\Delta H_{\mathrm{ads}} = 85.1\,\mathrm{kJ\,mol^{-1}} - 117.2\,\mathrm{kJ\,mol^{-1}}\theta_{*\mathrm{OCH_3}} \qquad \text{for Ni(111)} \tag{6}$$

At this coverage, the heats of adsorption are 81 kJ mol^{-1} on Ni(111) and 78 kJ mol^{-1} on Pt(111). The original values reported in the literature are 70 kJ mol^{-1} for Ni(111)[S7] and 74 kJ mol^{-1} [S2] (including a correction of 2 kJ mol^{-1} as explained in ref. S6).

2 DFT Data

The DFT single-point energies (SPE), zero-point energies (ZPE), and vibrational frequencies for Ni(111) are provided in Table S3. DFT results with the BEEF-vdW exchange-correlation functional for the adsorbates on the MgO(100) surface are listed in Table S5. The DFT results with the BEEF-vdW exchange-correlation functional for the Pt(111) slab are reported in the supporting information of ref. S10.

Table S3: Energies and vibrational frequencies obtained for adsorbates on Ni(111) from DFT calculations with the BEEF-vdW exchange-correlation functional.

No.	Species	SPE (eV)	ZPE (eV)	ν (cm^{-1})
1	$*OCH_3$	-94047.348	1.117	12, 141, 154, 308, 310, 350, 995, 1146, 1150, 1445, 1466, 1467, 2975, 3055, 3056
2	$*OH$	-93755.750	0.343	239, 243, 381, 475, 477, 3720
3	H_2O*	-93772.370	0.635	33, 79, 90, 158, 442, 454, 1590, 3641, 3751
4	CH_3OH*	-94063.8168	1.429	60, 118, 153, 172, 186, 215, 466, 958, 1054, 1147, 1324, 1445, 1468, 1478, 2985, 3059, 3108, 3661
5	$*O$	-93738.985	0.076	377, 378, 475

Table S4: DFT energies and vibrational frequencies of adsorbates on the MgO(100) (4x4) cell using the Γ-point and the BEEF-vdW exchange-correlation functional.

No.	Species	SPE (eV)	ZPE (eV)	ν (cm^{-1})
1	CH_4*	-323472.439	1.236	12, 12, 77, 91, 108, 290, 1323, 1329, 1349, 1544, 1546, 2986, 3095, 3097, 3106
2	C_2H_6*	-323764.305	2.030	12, 12, 12, 55, 88, 291, 311, 818, 858, 975, 1204, 1206, 1393, 1403, 1482, 1487, 1492, 1502, 2989, 2995, 3034, 3036, 3059, 3069
3	C_3H_8*	-324056.231	2.791	12, 12, 12, 12, 103, 209, 244, 275, 372, 758, 865, 902, 922, 1037, 1159, 1191, 1304, 1350, 1380, 1406, 1470, 1474, 1480, 1495, 1504, 2976, 2982, 2989, 3003, 3030, 3043, 3045, 3059
4	n-$C_4H_{10}*$	-324348.1716	3.568	12, 12, 63, 76, 123, 155, 218, 224, 272, 329, 425, 735, 805, 830, 956, 973, 1003, 1047, 1148, 1189, 1273, 1305, 1316, 1366, 1391, 1395, 1462, 1470, 1479, 1484, 1489, 1501, 2959, 2971, 2974, 2981, 2984, 3004, 3036, 3039, 3040, 3062

Continued on next page ...

Table S4 – continued from previous page

No.	Species	SPE (eV)	ZPE (eV)	ν (cm^{-1})
5	n-C_6H_{14}*	-324932.063	5.094	12, 12, 49, 57, 90, 132, 144, 150, 180, 228, 257, 281, 308, 372, 471, 728, 744, 802, 876, 896, 897, 995, 1003, 1035, 1049, 1062, 1141, 1186, 1233, 1259, 1288, 1313, 1319, 1327, 1366, 1371, 1389, 1395, 1462, 1463, 1470, 1476, 1481, 1486, 1489, 1499, 2952, 2958, 2962, 2969, 2970, 2978, 2982, 2984, 2995, 3013, 3040, 3043, 3047, 3054
6	n-C_8H_{18}*	-325515.946	6.613	12, 12, 14, 42, 87, 95, 112, 115, 150, 157, 177, 196, 239, 253, 258, 319, 348, 466, 474, 720, 740, 756, 796, 871, 875, 891, 950, 987, 993, 1026, 1031, 1043, 1048, 1082, 1133, 1182, 1216, 1235, 1261, 1287, 1297, 1307, 1319, 1321, 1331, 1361, 1369, 1372, 1391, 1392, 1461, 1462, 1465, 1471, 1477, 1479, 1482, 1486, 1492, 1498, 2946, 2949, 2955, 2959, 2962, 2965, 2967, 2974, 2976, 2978, 2986, 2992, 3001, 3019, 3040, 3045, 3048, 3056
7	MgO(100)	-323146.800	N/A	N/A

3 CBH for adsorbates on transition metal surfaces

Figure S1 shows the convergence of the enthalpy of formation of methoxy on Pt(111) and Ni(111) derived with the isodesmic and adsorption reaction as a function of the k-point density. For methoxy on Pt(111), the results are converged to within $1\,kJ\,mol^{-1}$ at the (2×2×1) k-point grid of the value with the (5×5×1) k-points. Additionally, the deviations at the Γ-point are also much lower for the isodesmic reaction compared to the adsorption reaction approach. Results on Ni(111) are similar, but both methods are converged to within $1\,kJ\,mol^{-1}$ at the (2×2×1) k-point mesh.

4 CBH for n-alkanes on MgO(100)

The error-cancellation reactions of the connectivity-based hierarchy for the n-alkanes on the MgO(100) surface are summarized in Table S5. Figure S2 shows the results from the benchmark of the enthalpies of formation of the n-alkanes on the MgO(100) facet.

To investigate the impact of the k-point grid on the computed enthalpies of formation via the conventional and the error cancellation approach, we performed additional relaxations for the MgO(100) slab with a (5×5×1) k-point grid. The single-point energies of the optimized structures are summarized in Table S6. Structures did not differ significantly from the Γ-point results, and we, therefore, used the ZPE energies from the Γ-point in Table S4.

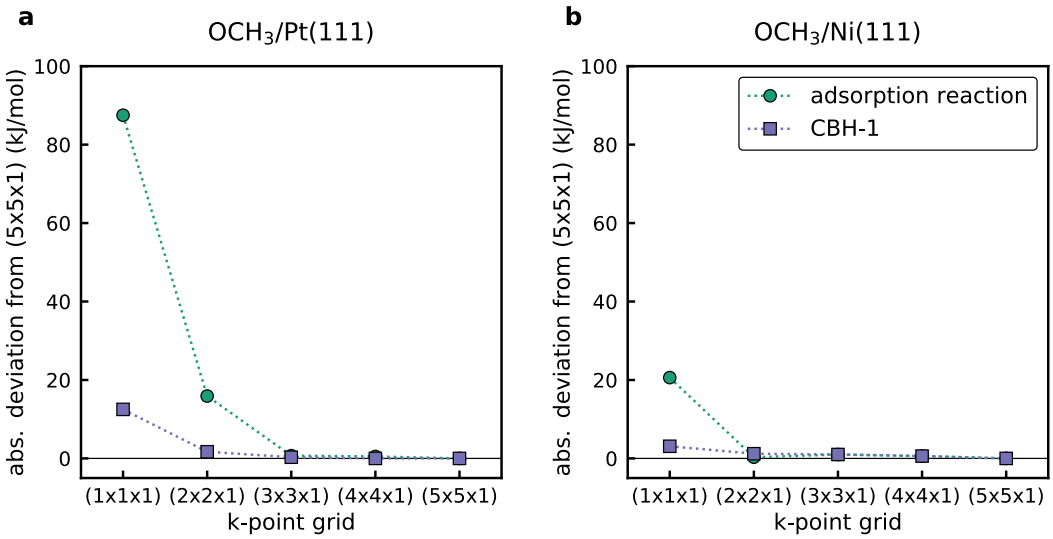

Figure S1: Convergence of the enthalpy of formation determined via the adsorption reaction approach and CBH method for methoxy adsorbed on a) Pt(111) and b) Ni(111). Note that the enthalpies of formation derived via the adsorption and isodesmic reaction are different.

Table S5: Referencing reactions to determine the enthalpies of formation of C_3H_8*, n-$C_4H_{10}*$, n-$C_6H_{14}*$, and n-$C_8H_{18}*$ on MgO(100) using the connectivity-based hierarchy for adsorbates.

Species	Reaction
C_3H_8*	$2\,C_2H_6* - CH_4* \xrightarrow{\text{CBH-1}} C_3H_8*$
n-$C_4H_{10}*$	$3\,C_2H_6* - 2\,CH_4* \xrightarrow{\text{CBH-1}}$ n-$C_4H_{10}*$
n-$C_4H_{10}*$	$2\,C_3H_8* - C_2H_6* \xrightarrow{\text{CBH-2}}$ n-$C_4H_{10}*$
n-$C_6H_{14}*$	$5\,C_2H_6* - 4\,CH_4* \xrightarrow{\text{CBH-1}}$ n-$C_6H_{14}*$
n-$C_6H_{14}*$	$4\,C_3H_8* - 3\,C_2H_6* \xrightarrow{\text{CBH-2}}$ n-$C_6H_{14}*$
n-$C_6H_{14}*$	$3\,$n-$C_4H_{10}* - 2\,C_3H_8* \xrightarrow{\text{CBH-3}}$ n-$C_6H_{14}*$
n-$C_8H_{18}*$	$7\,C_2H_6* - 6\,CH_4* \xrightarrow{\text{CBH-1}}$ n-$C_8H_{18}*$
n-$C_8H_{18}*$	$6\,C_3H_8* - 5\,C_2H_6* \xrightarrow{\text{CBH-2}}$ n-$C_8H_{18}*$
n-$C_8H_{18}*$	$5\,$n-$C_4H_{10}* - 4\,C_3H_8* \xrightarrow{\text{CBH-3}}$ n-$C_8H_{18}*$

The results for the two different k-point grids for the adsorbates are shown in Figure S3. Deviations between the Γ-point and (5×5×1) DFT energies are on the order of 2 kJ mol^{-1} for the adsorption reaction approach. Results from the CBH reactions differ only by 2 kJ mol^{-1}, which demonstrates that the usage of a Γ-point k-point grid is sufficient for this study.

In this study, we only performed the relaxation of the adsorbates for the BEEF-vdW functional. To evaluate the performance of the other exchange-correlation functionals, we calcu-

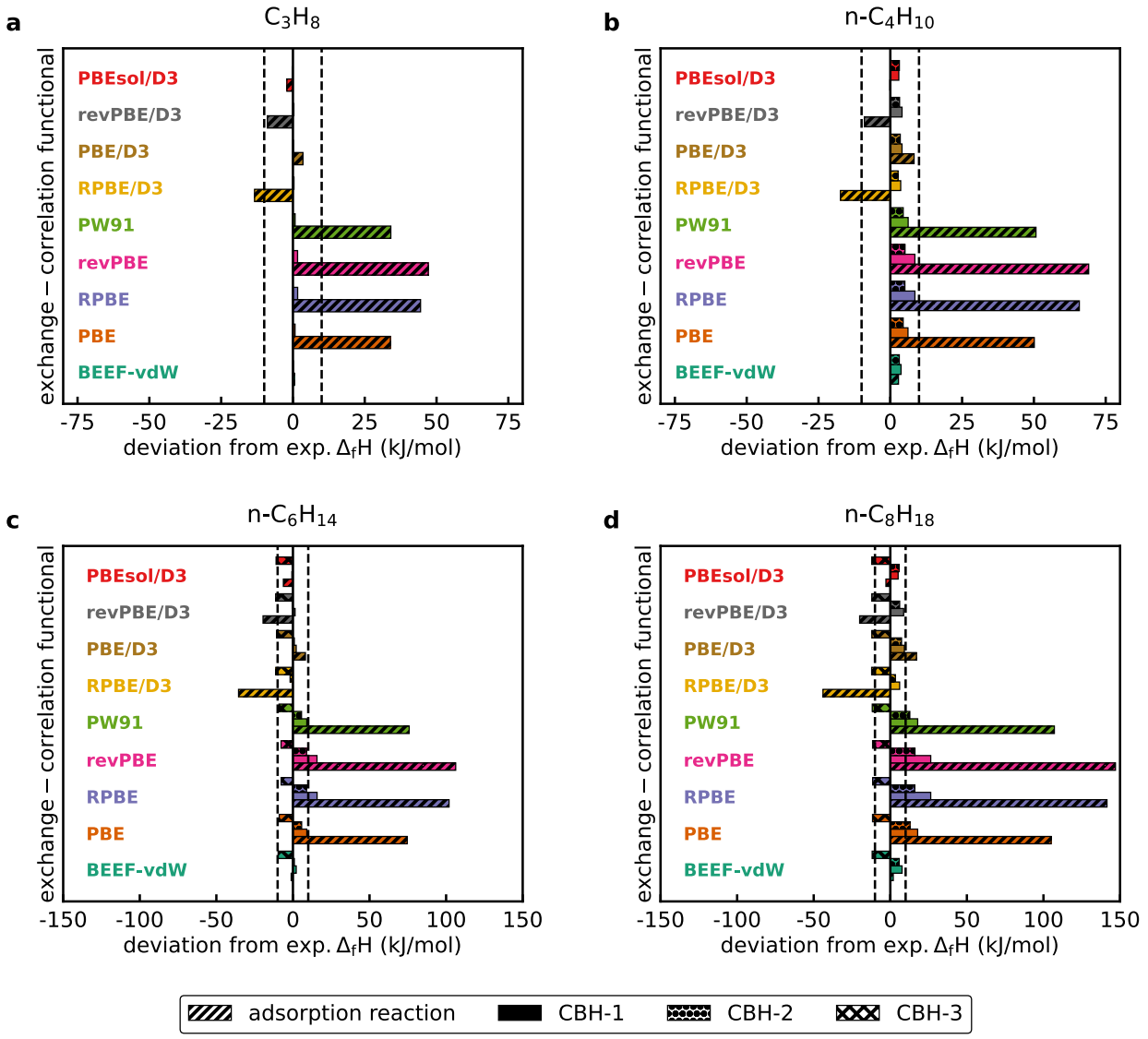

Figure S2: Comparison of computed and experimental enthalpies of formation of a) n-C_4H_{10}*, b) n-C_4H_{10}*, c) n-C_6H_{14}*, and d) n-C_8H_{18}* on MgO(100) using the conventional adsorption reaction approach and the error cancellation reactions of the connectivity-based hierarchy. Experimental enthalpies of adsorption are reported in the manuscript.

lated single-point energies for the optimized structures of the BEEF-vdW functional. This approach is a simplification to reduce computational cost, but it can potentially skew the results from functionals other than BEEF-vdW. To investigate the effect of this simplification, we performed optimization of propane and butane on a (2x2) slab for the PBE functional. The raw DFT data is summarized in Table S7.

Figure S4 compares the enthalpies of formation for C_3H_8* and n-C_4H_{10}* on MgO(100) for the (2x2) supercell derived with the structures optimized with the PBE functional and with the BEEF-vdW structure and the PBE single-point energy. There are differences between the optimized and non-optimized structure of 5 kJ mol^{-1} for the adsorption reaction approach

Table S6: DFT energies of the large MgO(100) (4x4) slab using a (5×5×1) k-point grid.

No.	Species	SPE (eV)
1	CH_4*	-323472.452
2	C_2H_6*	-323764.319
3	C_3H_8*	-324056.245
4	n-C_4H_{10}*	-324348.185
5	n-C_6H_{14}*	-324932.077
6	n-C_8H_{18}*	-325515.959
7	MgO(100)	-323146.800

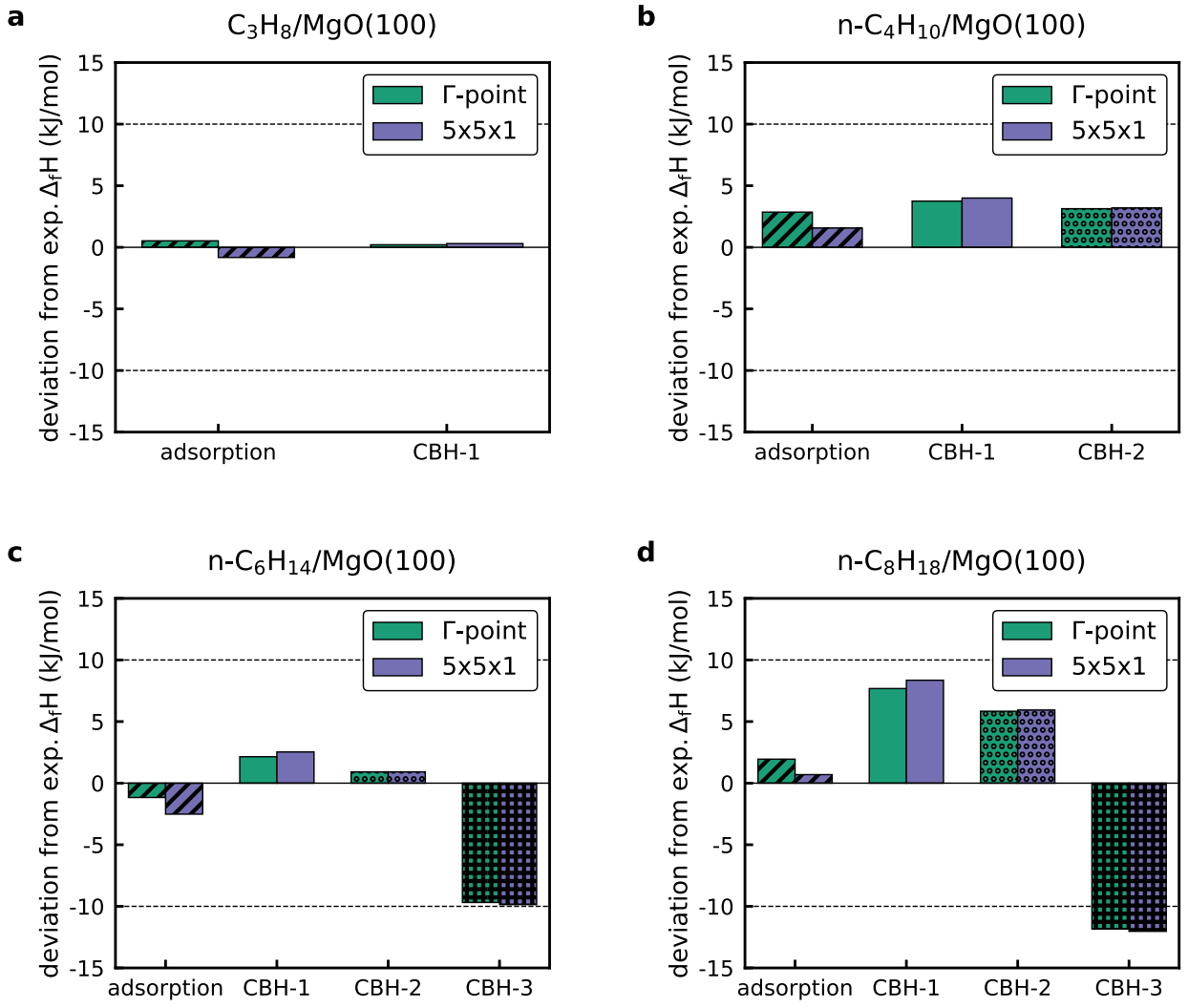

Figure S3: Effect of k-point grid on the predicted enthalpies of formation for a) propane, b) n-butane, c) n-hexane, and d) n-octane on MgO(100).

for propane. Using isodesmic reactions, these differences are reduced to 1 kJ mol^{-1}. A similar

Table S7: Summary of the DFT PBE data of the adsorbed n-alkanes on a MgO(100) (2x2) slab.

No.	Species	SPE (eV)	ZPE (eV)	ν (cm^{-1})
1	CH_4*	-80121.204	1.213	12, 12, 56, 60, 70, 295, 1274, 1279, 1314, 1503, 1509, 2959, 3073, 3078, 3090
2	C_2H_6*	-80404.372	1.983	12, 12, 12, 51, 65, 80, 304, 801, 803, 986, 1177, 1178, 1360, 1369, 1448, 1449, 1452, 1454, 2957, 2960, 3008, 3013, 3033, 3039, 3039
3	C_3H_8*	-80687.596	2.745	12, 35, 42, 59, 65, 76, 220, 262, 356, 731, 860, 881, 900, 1045, 1137, 1170, 1278, 1322, 1347, 1364, 1433, 1438, 1443, 1452, 1459, 2943, 2952, 2955, 2970, 3011, 3020, 3026, 3028
4	n-C_4H_{10}*	-80970.823	3.493	12, 12, 25, 50, 71, 82, 134, 217, 250, 256, 414, 713, 784, 822, 929, 947, 1000, 1049, 1132, 1165, 1244, 1274, 1286, 1337, 1355, 1356, 1429, 1434, 1442, 1446, 1449, 1455, 2932, 2942, 2953, 2954, 2956, 2978, 3016, 3020, 3027, 3027
7	MgO(100)	-79805.461	N/A	N/A

trend is obtained for butane. There are slightly larger deviations for the adsorption reaction approach. Enthalpies of formation determined via CBH-1 or CBH-2 differ only by a few $kJ\,mol^{-1}$ and are in good agreement with the experimental value. Overall, there are small differences between the results for the PBE-optimized structure and when using the BEEF-vdW structure with the PBE single-point energies. However, the conclusions that can be drawn from the simplified approximation are still valid and not fundamentally changed when optimizing the structure with the exchange-correlation functional.

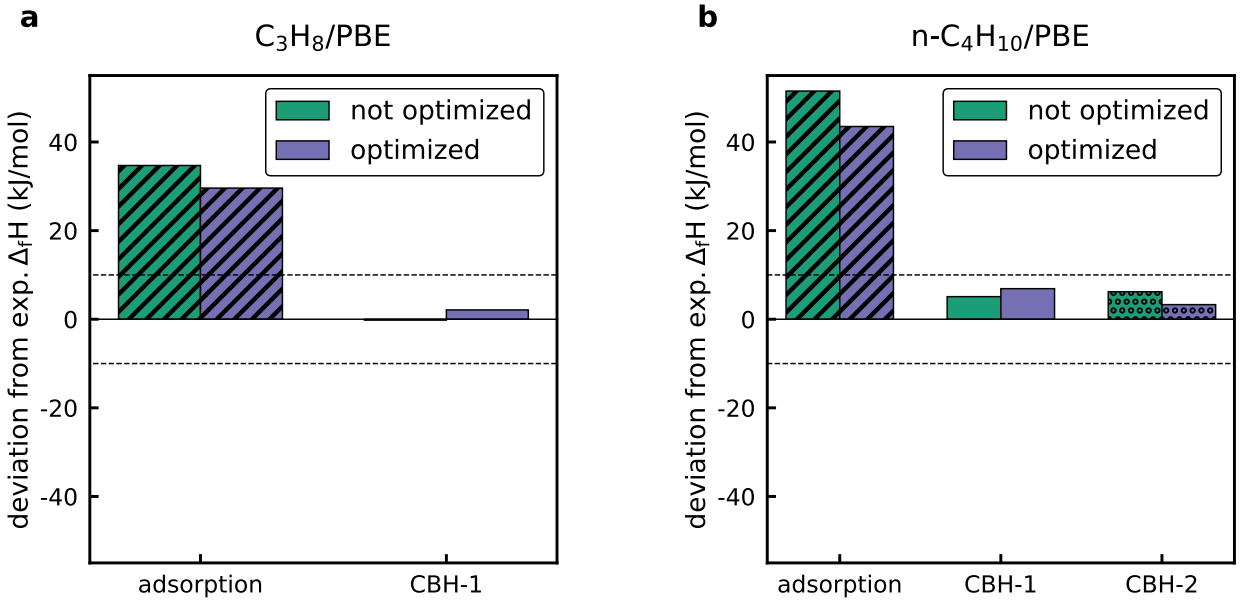

Figure S4: Comparison of the predicted enthalpies for the single-point energies determined with the PBE functional for the BEEF-vdW structure and the DFT energy of the optimized PBE structure for a) propane and b) n-butane on MgO(100).

References

(S1) Ruscic, B.; Bross, D. H. *Computer Aided Chemical Engineering*; Elsevier, 2019; Vol. 45; pp 3–114.

(S2) Karp, E. M.; Silbaugh, T. L.; Crowe, M. C.; Campbell, C. T. Energetics of Adsorbed Methanol and Methoxy on Pt(111) by Microcalorimetry. *J. Am. Chem. Soc.* **2012**, *134*, 20388–20395.

(S3) Abbas, N. M.; Madix, R. J. The Effects of Structured Overlayers of Sulfur on the Kinetics and Mechanism of Simple Reactions on Pt(111): I. Formaldehyde Decomposition. *Appl. Surf. Sci.* **1981**, *7*, 241–275.

(S4) Wellendorff, J.; Silbaugh, T. L.; Garcia-Pintos, D.; Nørskov, J. K.; Bligaard, T.; Studt, F.; Campbell, C. T. A Benchmark Database for Adsorption Bond Energies to Transition Metal Surfaces and Comparison to Selected DFT Functionals. *Surf. Sci.* **2015**, *640*, 36–44.

(S5) Karp, E. M.; Campbell, C. T.; Studt, F.; Abild-Pedersen, F.; Nørskov, J. K. Energetics of Oxygen Adatoms, Hydroxyl Species and Water Dissociation on Pt(111). *J. Phys. Chem. C* **2012**, *116*, 25772–25776.

(S6) Silbaugh, T. L.; Campbell, C. T. Energies of Formation Reactions Measured for Adsorbates on Late Transition Metal Surfaces. *J. Phys. Chem. C* **2016**, *120*, 25161–25172.

(S7) Carey, S. J.; Zhao, W.; Harman, E.; Baumann, A.-K.; Mao, Z.; Zhang, W.; Campbell, C. T. Energetics of Adsorbed Methanol and Methoxy on Ni(111): Comparisons to Pt(111). *ACS Catal.* **2018**, *8*, 10089–10095.

(S8) Kreitz, B.; Lott, P.; Bae, J.; Blöndal, K.; Angeli, S.; Ulissi, Z. W.; Studt, F.; Goldsmith, C. F.; Deutschmann, O. Detailed Microkinetics for the Oxidation of Exhaust Gas Emissions through Automated Mechanism Generation. *ACS Catal.* **2022**, *12*, 11137–11151.

(S9) Kreitz, B.; Kogekar, G.; Cheula, R.; Goldsmith, C. F. Structure-Dependent Microkinetic Modeling of the CO_2 Desorption with Surface Diffusion. *J. Catal.* **2025**, *452*, 116407.

(S10) Kreitz, B.; Abeywardane, K.; Goldsmith, C. F. Linking Experimental and *Ab Initio* Thermochemistry of Adsorbates with a Generalized Thermochemical Hierarchy. *J. Chem. Theory Comput.* **2023**, *19*, 4149–4162.